On the Role of the Atmospheric Energy Transport in 2 × CO_2–Induced Polar Amplification in CESM1

RUNE G. GRAVERSEN

Department of Physics and Technology, University of Tromsø, Tromsø, Norway

PETER L. LANGEN

Danish Meteorological Institute, Copenhagen, Denmark

(Manuscript received 22 August 2018, in final form 19 March 2019)

ABSTRACT

A doubling of the atmospheric CO_2 content leads to global warming that is amplified in the polar regions. The CO_2 forcing also leads to a change of the atmospheric energy transport. This transport change affects the local warming induced by the CO_2 forcing. Using the Community Earth System Model (CESM), the direct response to the transport change is investigated. Divergences of the transport change associated with a CO_2 doubling are implemented as a forcing in the 1 × CO_2 preindustrial control climate. This forcing is zero in the global mean. In response to a CO_2 increase in CESM, the northward atmospheric energy transport decreases at the Arctic boundary. However, the transport change still leads to a warming of the Arctic. This is due to a shift between dry static and latent transport components, so that although the dry static transport decreases, the latent transport increases at the Arctic boundary, which is consistent with other model studies. Because of a greenhouse effect associated with the latent transport, the cooling caused by a change of the dry static component is more than compensated for by the warming induced by the change of the latent transport. Similar results are found for the Antarctic region, but the transport change is larger in the Southern Hemisphere than in its northern counterpart. As a consequence, the Antarctic region warms to the extent that this warming leads to global warming that is likely enhanced by the surface albedo feedback associated with considerable ice retreat in the Southern Hemisphere.

1. Introduction

The atmospheric energy transport plays a crucial role for the climate at the high latitudes. This transport brings to the polar areas an amount of energy comparable to that provided directly by the sun (Oort and Peixóto 1983). Therefore a small variation at the polar boundary of this transport may affect the high-latitude climate considerably (Graversen 2006). It has also been argued that the atmospheric energy transport plays a role in climate change at the high latitudes (Cai 2005; Alexeev et al. 2005; Langen and Alexeev 2007; Ding et al. 2017); for instance, two studies suggest that change of the energy transport plays a major role for the strong winter warming of about 4°C observed in the Svalbard area over the past 20 years (Dahlke and Maturilli 2017; Isaksen et al. 2016).

The atmospheric energy transport can be decomposed into a dry static and a latent part, where the latter is associated with water vapor advection (Fig. 1). It has been acknowledged that the latent component may affect the Arctic more than its dry static counterpart (Koenigk et al. 2013; Graversen and Burtu 2016), and that the latent transport has a large effect on Arctic sea ice (Kapsch et al. 2013; Gong et al. 2017; S. Lee et al. 2017; H. J. Lee et al. 2017). The latent transport brings energy to the Arctic in form of water vapor that releases energy because of condensation. In addition the water vapor transport enhances the local Arctic greenhouse effect, both by the water vapor itself and through the increased cloudiness caused by the transport. Although clouds globally have a net cooling effect, they have a warming effect in the Arctic, except possibly for some

Corresponding author: Rune G. Graversen, rune.graversen@uit.no

DOI: 10.1175/JCLI-D-18-0546.1

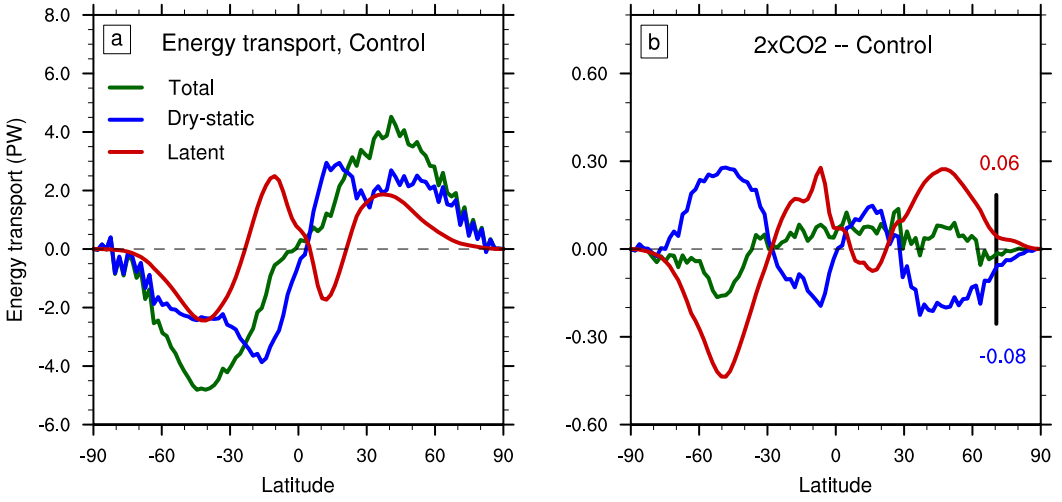

FIG. 1. (a) Meridional atmospheric transport of dry static, latent, and total energy in the preindustrial control experiment and (b) their changes due to a doubling of CO_2. Numbers in (b) indicate changes at 70° N in units of PW. The transports and their changes are 59-yr climatologies of transport quantities calculated based on all model hybrid levels and time steps.

summer months (Intrieri et al. 2002). It has also been shown that intrusions of water vapor into the Arctic during winter induce Arctic warming and sea ice melt events (Woods et al. 2013; Yang and Magnusdottir 2017), and that these intrusions are increasing in frequency during the past two decades causing trends in both temperature and sea ice, especially in the Barents and Kara Sea areas (Woods and Caballero 2016). In addition, anomalously low Arctic sea ice extent in September is linked to latent energy transport during spring (Kapsch et al. 2013), partly because the spring latent energy transport affects the melt onset; early melt onset in the Arctic is proceeded by anomalously large latent energy transport convergence (Mortin et al. 2016).

Climate models indicate that anthropogenically induced climate change alters the energy transport so that the total transport remains almost unchanged at the Arctic boundary, but the dry static transport decreases whereas the latent transport increases (Hwang et al. 2011; Kay et al. 2012; Skific and Francis 2013; Koenigk et al. 2013; Bengtsson et al. 2013). It has been argued that this shift between the two transport components may lead to Arctic warming although the total transport decreases (Graversen and Burtu 2016; Yoshimori et al. 2017). Many models show that the changes of the two components are on the order of 10% over the twenty-first century for the ''business-as-usual'' scenarios A2 (Hwang et al. 2011) and RCP8.5 (Koenigk et al. 2013), which may potentially lead to a significant climate impact of the energy transport.

Here we attempt to separate the effect of energy transport change in the climate response to forcing: By using a state-of-the-art climate model, the energy transport change due to a doubling of the atmospheric CO_2 content is estimated. Then divergences of the energy transport change are applied to the model as a forcing. As far as is known to the authors, this is the first attempt to design such climate model experiments for separating the effect of the energy transport in $2 \times CO_2$ forcing. The advantage with such experiments is that the effect of the energy transport can be isolated. However, the experiments are complicated to design, include subjective choices, and are by construction artificial, which will be discussed in the latter sections. Climate-model experiments for separating the effect of changes of specific processes have previously been conducted in order to study, for example, the surface albedo feedback (Hall 2004; Graversen and Wang 2009; Mauritsen et al. 2013; Graversen et al. 2014), water vapor feedback (Schneider et al. 1999; Hall and Manabe 1999; Langen et al. 2012; Mauritsen et al. 2013), cloud feedback (Vavrus 2004; Langen et al. 2012; Mauritsen et al. 2013), and the lapse-rate feedback (Graversen et al. 2014). Such studies are based on online approaches where the models are designed to neglect a given feedback process, or to include only that particular process. Other indirect methods have been applied to investigate the climate effect of feedbacks and climate processes. These indirect, offline methods are often based on running the radiation code stand-alone for atmospheres perturbed to represent the effect of a given feedback or climate process. Such methods include the partial radiative perturbation (RPM) method (Wetherald and Manabe 1988) and the radiative kernel method (Soden et al. 2008).

2. Methods

The fundamental idea of this work is to investigate the climate effect of a change in the atmospheric energy transport due to a forcing by a doubling of the atmospheric CO_2 content. The study is based on a state-of-the-art climate model, the Community Earth System Model (CESM) from National Center for Atmospheric Research (NCAR), Boulder, Colorado. First, the change of the energy transport due to a CO_2 doubling ($2 \times CO_2 - 1 \times CO_2$) is derived. Then divergences as a function of height of this transport change are used as a forcing of the control ($1 \times CO_2$) climate.

a. Climate model description

The Community Earth System Model, version 1.2 (CESM1; Hurrell et al. 2013), is used in a slab-ocean model (SOM) configuration. The model's atmospheric component is the Community Atmospheric Model, version 5 (CAM5; Neale et al. 2012). It is applied using a finite-volume dynamical core, 29 hybrid levels, a time step of 30 min, and an ~2° horizontal resolution. The ocean part includes an isothermal mixed layer only, with a fixed horizontal transport of energy. The horizontal ocean energy transport convergences in SOM, often referred to as the q fluxes, are determined from the climatology of an equilibrium run including a full dynamical ocean model. The q fluxes are given as the climatological mean of the imbalance between the ocean mixed layer energy change, and the energy flux into the ocean across the atmosphere–ocean and ice–ocean interface and from river discharge (Bitz et al. 2012; Graversen et al. 2014). The q fluxes as well as the depth of the mixed layer are based on the climatology from the last 70 years of a control run with a full coupled version of the model. This control run has been run to preindustrial climate equilibrium on an NCAR machine, and for additionally 100 model years at the local machine used for this work.

To obtain the energy transport change associated with a CO_2 doubling, SOM is run in a $1 \times CO_2$ and a $2 \times CO_2$ configuration with the atmospheric CO_2 level set to 284.7 and 569.4 ppm, respectively, where the former represents the preindustrial conditions. The climate effect due to an energy transport change associated with a CO_2 doubling is derived by implementing divergences of the transport change as a forcing into the $1 \times CO_2$ control configuration.

b. Energy equations

An energy equation for dry static and kinetic energy for a unit mass of atmospheric air can be developed by combing the first law of thermodynamics, the momentum equation, the continuity equation, the equation of state of an ideal gas, and the hydrostatic approximation. Following, for example, Kasahara [1974, Eq. (5.7)], and ignoring source and sink terms associated with diabatic warming and cooling, frictional dissipation, and molecular diffusion, this equation in pressure coordinates can be written

$$\left(\frac{\partial}{\partial t}[k + c_p T]\right)_p = -\nabla_p \cdot [(k + c_p T + gz)\mathbf{v}] - \frac{\partial}{\partial p}[(k + c_p T + gz)\omega]. \tag{1}$$

Here t is time, z is height, T is temperature, p is pressure, g is gravity, $\mathbf{v}$ is the horizontal wind vector, $\omega = dp/dt$ is the vertical velocity in pressure coordinates, $k = \mathbf{v}^2/2$ is the specific kinetic energy, c_p is the specific heat capacity at constant pressure, and $(\partial/\partial t)_p$ and ∇_p are time derivative and horizontal derivative vector, respectively, at a constant pressure surface. To obtain an expression for the energy change at a given model hybrid level η_n, where η is the vertical hybrid coordinate, and n is a level index increasing upward, we integrate Eq. (1) between adjacent half levels with indices $n - 1/2$ and $n + 1/2$ and pressure $p_{n-1/2}$ and $p_{n+1/2}$. Integration between these hybrid half levels and interchanging the order of differentiation and integration taking into account that $p_{n+1/2}$ and $p_{n-1/2}$ may be functions of time and horizontal space (by using Leibniz's integration rule) yield

$$\frac{\partial}{\partial t}\int_{p_{n+1/2}}^{p_{n-1/2}}(k + c_p T)\frac{dp}{g} = \underbrace{-\nabla \cdot \int_{p_{n+1/2}}^{p_{n-1/2}}(k + c_p T + gz)\mathbf{v}\frac{dp}{g}}_{\text{I}} + \underbrace{\frac{1}{g}[(k + c_p T + gz)\omega]_{n+1/2} - \frac{1}{g}[(k + c_p T + gz)\omega]_{n-1/2}}_{\text{II}}$$

$$+ \underbrace{\frac{1}{g}[k + c_p T]_{n-1/2}\frac{\partial p_{n-1/2}}{\partial t} - \frac{1}{g}[k + c_p T]_{n+1/2}\frac{\partial p_{n+1/2}}{\partial t}}_{\text{III}} + \underbrace{\frac{1}{g}[(k + c_p T + gz)\mathbf{v}]_{n-1/2} \cdot \nabla p_{n-1/2} - \frac{1}{g}[(k + c_p T + gz)\mathbf{v}]_{n+1/2} \cdot \nabla p_{n+1/2}}_{\text{III}} \cdot \tag{2}$$

Here $[a]_n$ indicates a taken at hybrid level n. Equation (2) states that the energy change per unit area in a grid cell between two hybrid half levels is due to horizontal divergence of energy advection (term I), vertical energy advection (terms II), and contribution from temporal change of the upper and lower pressure boundaries of the grid cell, and horizontal flux across these boundaries (terms III).

For latent energy, a similar conservation equation as for the dry static plus kinetic energy [Eq. (1)] can be stated. Again ignoring sources and sink terms associated with evaporation and condensation and molecular diffusion, this equation yields

$$\left(\frac{\partial}{\partial t}[Lq]\right)_p = -\nabla_p \cdot [Lq\mathbf{v}] - \frac{\partial}{\partial p}[Lq\omega], \tag{3}$$

where q is specific humidity and L is latent heat of condensation. Integration between hybrid half levels with indices $n + 1/2$ and $n - 1/2$ gives

$$\frac{\partial}{\partial t}\int_{p_{n+1/2}}^{p_{n-1/2}} Lq\frac{dp}{g} = \underbrace{-\nabla \cdot \int_{p_{n+1/2}}^{p_{n-1/2}} Lq\mathbf{v}\frac{dp}{g}}_{\text{I}} + \underbrace{\frac{1}{g}[Lq\omega]_{n+1/2} - \frac{1}{g}[Lq\omega]_{n-1/2}}_{\text{II}} + \underbrace{\frac{1}{g}[Lq]_{n-1/2}\frac{\partial p_{n-1/2}}{\partial t} - \frac{1}{g}[Lq]_{n+1/2}\frac{\partial p_{n+1/2}}{\partial t}}_{\text{III}}$$

$$+\underbrace{\frac{1}{g}[Lq\mathbf{v}]_{n-1/2} \cdot \nabla p_{n-1/2} - \frac{1}{g}[Lq\mathbf{v}]_{n+1/2} \cdot \nabla p_{n+1/2}}_{\text{III}}, \tag{4}$$

where the terms have the same meaning as for the dry static energy conservation in Eq. (2). Note that all terms in both Eqs. (2) and (4) are in the units of watts per square meter.

VERTICAL FLUXES AND BOUNDARY TERMS

Here it will be argued that for the present study, vertical fluxes and interface terms [terms II and III in Eqs. (2) and (4)] should be taken into account when it comes to applying forcing based on the dry static transport change, whereas they should be ignored for the forcing of the latent part.

In pressure coordinates, and in hydrostatic balance, the vertical mass flux (along a p axis), ω/g, at a given hybrid level η_n is given by

$$\begin{aligned}\frac{1}{g}\omega_n &= \frac{1}{g}\left[\frac{dp}{dt}\right]_n \\ &= \frac{1}{g}\left[\left(\frac{\partial p}{\partial t}\right)_\eta + \mathbf{v} \cdot \nabla_\eta p + \dot{\eta}\frac{\partial p}{\partial \eta}\right]_n \\ &= \frac{1}{g}\left(\frac{\partial p_n}{\partial t} + \mathbf{v}_n \cdot \nabla p_n + \left[\dot{\eta}\frac{\partial p}{\partial \eta}\right]_n\right),\end{aligned} \tag{5}$$

where an expansion of the total derivative in hybrid coordinates is applied for the second equality. The last term on the rhs is the mass flux through the hybrid surface along the η axis, whereas the two first terms on the rhs are associated with the temporal pressure change at the hybrid surface and the horizontal flux along the pressure gradient at that surface, respectively. Hence Eq. (5) states that the mass flux at a given hybrid surface is equal to the mass flux through that surface plus contributions from the change and horizontal gradient of the pressure at the hybrid surface.

Applying Eq. (5) on the hybrid levels $n + 1/2$ and $n - 1/2$, multiplying with $k + c_pT + gz$ or Lq taken at the same hybrid levels, and setting into Eqs. (2) and (4), respectively, yield

$$\begin{aligned}\frac{\partial}{\partial t}\int_{p_{n+1/2}}^{p_{n-1/2}}(k + c_pT)\frac{dp}{g} &= -\nabla \cdot \int_{p_{n+1/2}}^{p_{n-1/2}}(k + c_pT + gz)\mathbf{v}\frac{dp}{g} \\ &\quad + \frac{1}{g}\left[(k + c_pT + gz)\left(\dot{\eta}\frac{\partial p}{\partial \eta}\right)\right]_{n+1/2} \\ &\quad - \frac{1}{g}\left[(k + c_pT + gz)\left(\dot{\eta}\frac{\partial p}{\partial \eta}\right)\right]_{n-1/2} \\ &\quad + \frac{1}{g}[gz]_{n+1/2}\frac{\partial p_{n+1/2}}{\partial t} \\ &\quad - \frac{1}{g}[gz]_{n-1/2}\frac{\partial p_{n-1/2}}{\partial t},\end{aligned} \tag{6}$$

and

$$\begin{aligned}\frac{\partial}{\partial t}\int_{p_{n+1/2}}^{p_{n-1/2}} Lq\frac{dp}{g} &= -\nabla \cdot \int_{p_{n+1/2}}^{p_{n-1/2}} Lq\mathbf{v}\frac{dp}{g} + \frac{1}{g}\left[Lq\left(\dot{\eta}\frac{\partial p}{\partial \eta}\right)\right]_{n+1/2} \\ &\quad - \frac{1}{g}\left[Lq\left(\dot{\eta}\frac{\partial p}{\partial \eta}\right)\right]_{n-1/2}.\end{aligned} \tag{7}$$

Hence in this form, energy change in a hybrid grid cell per unit area is due to horizontal energy transport divergence, energy flux across the vertical boundaries,

and, for the case of dry static energy, change of potential energy associated with changes of the mass of the grid cell as the pressure at the vertical boundaries changes.

In the present study the intention is to investigate the climate effect of local energy change [lhs of Eqs. (6) and (7)] due to a change of the horizontal energy advection (first term on the rhs of these equations). A change in the vertical advection includes climate effects due to the lapse-rate feedback (Hansen et al. 1984): For instance, a large contribution to the lapse-rate feedback is associated with an increase in vertical advection of water vapor in the tropics causing an increase in condensation and latent heat release at the upper-tropospheric levels, which leads to more efficient radiation to space and cooling of the Earth system. Mainly for that reason the lapse-rate feedback is believed to be negative in a global mean (e.g., Graversen et al. 2014). In the present study, the focus is on the effect of changes of the horizontal energy advection, and changes of vertical fluxes will therefore be ignored for the latent energy advection [Eq. (7)].

However, when it comes to dry static energy conservation, the horizontal and vertical energy fluxes are intrinsically linked: For instance, convergence of heat in the troposphere will rapidly be felt in the stratosphere since potential energy gz in the stratosphere will increase because of thermal expansion in the troposphere. This affects the horizontal energy advection in the stratosphere even in the case where no change in vertical mass fluxes has occurred at the boundary between the troposphere and the stratosphere. However, the stratospheric horizontal advection changes will still be in accordance with vertical energy transport changes at the tropopause, since although the mass flux across the tropopause may be unaltered, the potential energy gz at this interface increases leading to an increase of the vertical energy advection. To see this, Fig. 2a shows the $2 \times CO_2$–induced change in energy transport divergence as a function of height and averaged over the Arctic. For the dry static part, large divergences are found in the troposphere whereas convergences are apparent in the stratosphere. However, when taking into account vertical fluxes and the terms associated with hybrid level changes and gradients [last four terms in Eq. (6), or terms II and III in Eq. (2)], the stratospheric changes almost vanish (Fig. 2d). Hence the stratospheric horizontal divergences, which are of considerable magnitudes, appear to be mostly a result of the vertical fluxes and terms associated with pressure changes and horizontal pressure gradients of the hybrid levels, rather than leading to actual warming and energy increase of the stratosphere.

As apparent from Fig. 2, the intrinsic linkage between horizontal and vertical advection, as it appears for the dry static energy, is only a negligible issue when it comes to the latent energy. To avoid forcings associated with the lapse-rate feedback, it was therefore decided to not include the vertical advection terms and interface terms for the latent energy transport forcing; hence for this forcing only the horizontal advection term was included [term I in Eq. (4)]. And we decided to include these terms [terms II and III in Eq. (2)] for the dry static transport forcing because of the above-mentioned linkage to the horizontal advection that would otherwise lead to unrealistic forcings, for example, in the stratosphere.

c. *Experimental design*

The following provides a description of the methods used to extract the energy transport from the model, and to implement changes of the energy transport as a forcing. The kinetic energy transport is several orders of magnitudes smaller than the dry static energy (Oort and Peixóto 1983) and has been ignored in this work.

1) DIVERGENCES OF THE ENERGY TRANSPORT CHANGE

In SOM, the horizontal energy transport at each model level [integrals in term I in Eqs. (2) and (4)] is calculated online at each model time step of 30 min and outputted as monthly means, both for the $1 \times CO_2$ preindustrial control climate and for the $2 \times CO_2$ climate. Figure 1a shows a 59-yr climatology of the vertically integrated and zonally and annually averaged transport in the $1 \times CO_2$ climate, and Fig. 1b provides the corresponding climatology of the changes due to a CO_2 doubling.

Monthly mean divergences of the transport are calculated offline by applying a horizontal divergence operator on the monthly mean output of the transports. Note that divergence operator and time integral can here be interchanged. The 59-yr climatology for the Arctic of these divergences as a function of height is shown in Fig. 2a.

In addition, as mentioned above, it was decided for the dry static part to take into account the vertical energy fluxes. Since the mass flux *at* the hybrid interface, $\boldsymbol{\omega}/g$, rather than the flux *through* it, $\dot{\eta}/g(\partial p/\partial \eta)$, is provided in the model, all terms II and III in Eq. (2) are calculated online in addition to term I. The temporal and horizontal derivatives of the pressure, which are included in the terms III, are not directly calculated in the model, but we developed code to extract these quantities from the

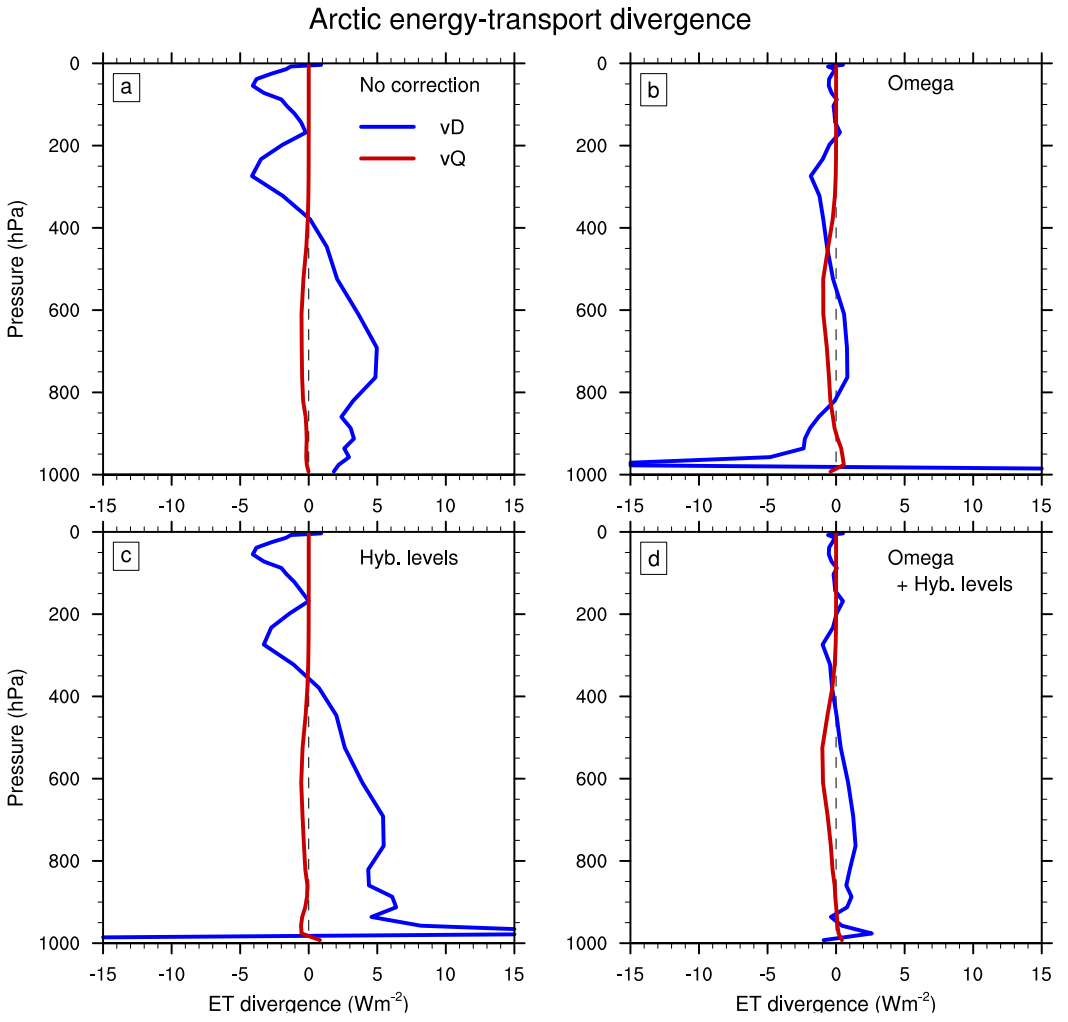

FIG. 2. Arctic (north of 70°N) changes due to a CO_2-doubling of (a) energy transport divergences [terms I in Eqs. (2) and (4)], (b) divergences plus vertical transport terms (terms I and II), (c) divergences plus hybrid-level interface terms (terms I and III), and (d) all terms (I, II, and III). The changes are decomposed into dry static and latent parts.

dynamical core following the method for computing $\boldsymbol{\omega}$ in the model. Hence, as for the horizontal transport, all these terms II and III are calculated online at each model time step and outputted as monthly means. As is apparent from a comparison of Eqs. (2) and (6), there is a cancellation between terms II and III. This is also evident from Figs. 2b and 2c, showing the addition of terms II and III, respectively, to the divergence term (term I). Especially in the lower part of the troposphere, where the pressure at the hybrid levels shows large temporal and spatial variability, there is a large cancellation between the effect of the two types of terms (Fig. 2d). In the stratosphere above ~180 hPa, the pressure at the hybrid levels is constant by construction. Hence at these levels terms III are all zero, and the mass flux at, $\boldsymbol{\omega}/g$, and through, $\dot{\eta}/g(\partial p/\partial \eta)$, these levels become equal, implying that only the terms II have an effect here (Fig. 2b).

2) FORCING DUE TO ENERGY TRANSPORT CHANGE

After having estimated the energy transport divergences, and their changes due to a CO_2 doubling, the idea is now to apply these divergence changes as a forcing in the $1 \times CO_2$ climate. Based on the discussion above, for the dry static part, all terms I–III on the rhs of Eq. (2) are applied as a forcing whereas for the latent part, only the term I of Eq. (4) is used. These constitute the "raw" forcing fields, which are climatologies with a monthly resolution and functions of three-dimensional space: latitude, longitude, and hybrid level.

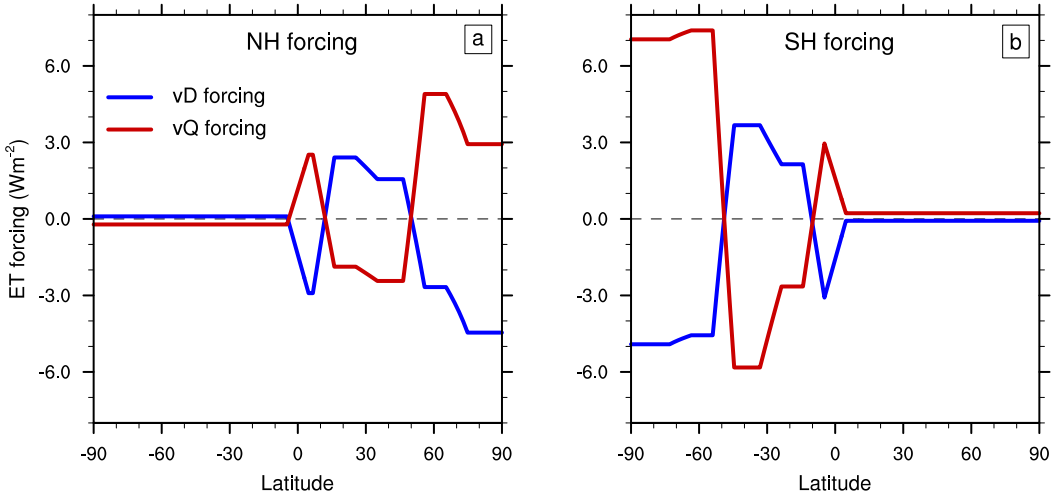

FIG. 3. Vertical integrals of forcings due to energy transport change associated with a CO_2 doubling for the experiment with forcing in the (a) NH only and (b) SH only. The forcings are shown for both the dry static (vD) and the latent (vQ) part.

As the long-term climatology of the energy transport shows a spatially noisy structure (Fig. 1), we decided to apply smoothed, area-average forcing fields. They are obtained as follows: 1) First the raw forcing fields are zonally and area-weighted meridionally averaged into 20° latitude bins, and 2) then an area-weighted latitude running-mean filter spanning ~8° latitude is applied on these bins.

Three experiments are conducted applying forcing in the Northern Hemisphere (NH forcing), in the Southern Hemisphere (SH forcing), and globally (Global forcing). In each of the three experiments it has been ensured that the total global forcing is zero by subtracting the globally averaged forcing from the lowest model level of the forcing fields. Finally, the monthly time resolution of the forcing fields is extrapolated into a daily resolution. These are the forcing fields that are applied in the model. The forcings as applied in the NH and SH forcing experiments are shown in a vertically integrated form in Fig. 3. The distribution of the forcings as a function of model level is shown in the form of transport divergences in Fig. 4 for the Arctic and NH midlatitudes for the NH forcing experiment. Note that the vertical sum of the divergences over all model levels given by the

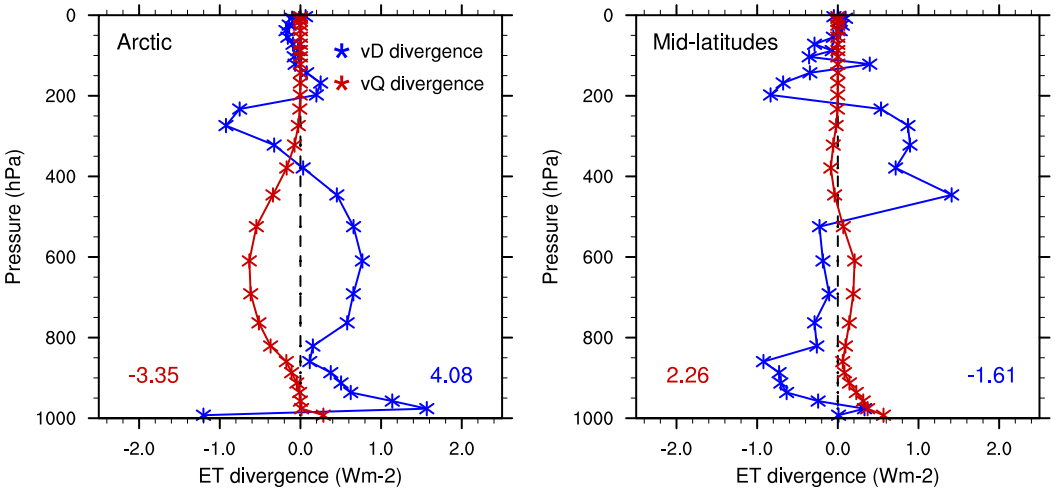

FIG. 4. Forcings in form of energy transport divergences due to transport change associated with a CO_2 doubling. Forcings are shown for each model level and for (left) the Arctic (north of 70° N) and (right) NH midlatitudes (30°–50°N). The forcings are shown for both the dry static (vD) and the latent (vQ) part. The numbers in the frames indicate the vertical sum of dry static (blue) and latent (red) divergences ($W\,m^{-2}$).

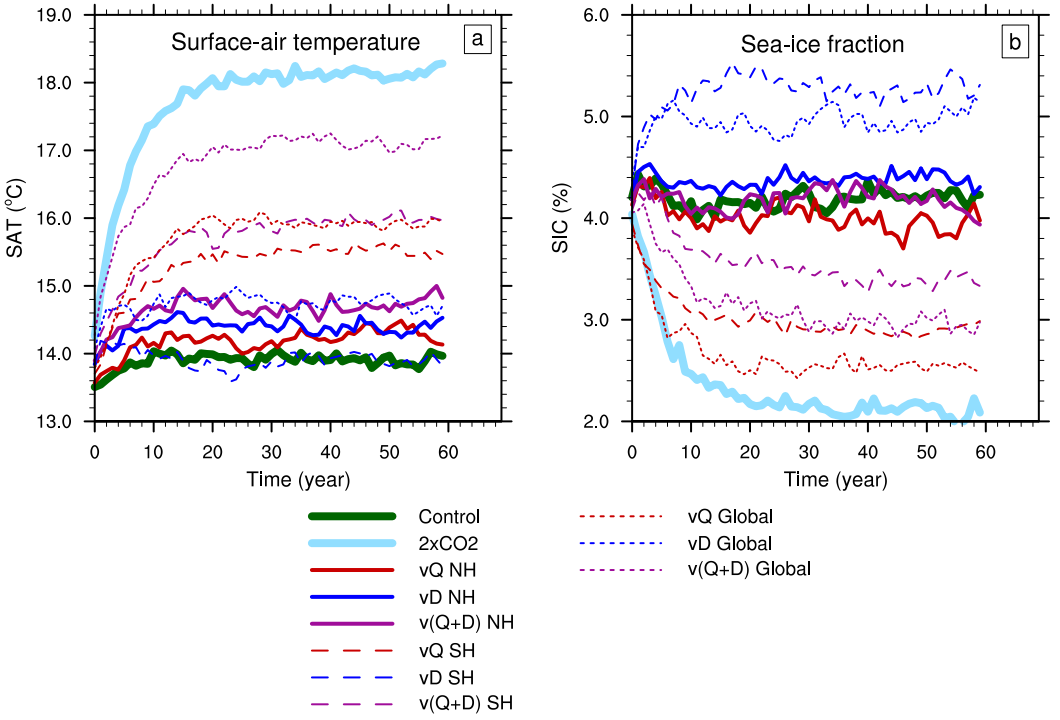

FIG. 5. Global-mean (a) 2-m temperature and (b) sea ice extent as a function of model year. The time series are shown for the $1 \times CO_2$ control experiment (Control), the doubling of CO_2 experiment ($2 \times CO_2$), and all experiments with forcings of the $1 \times CO_2$ climate with changes of energy transport divergences due to a CO_2 doubling. The latter experiments are combinations of NH, SH, and global forcing, and forcing from dry static (vD), latent (vQ), and total [v(Q + D)] transport divergence changes.

numbers in the frames of Fig. 4 constitutes −1 times the zonal-mean forcings shown in Fig. 3.

Finally note that the global means of instantaneous divergences and convergences of atmospheric energy transport add up to zero as the Earth atmosphere is a closed fluid dynamic system when it comes to dry mass. Hence applying such divergences and convergences as forcings induces a net zero global forcing. However, the smoothing of the forcings as indicated above, and the application of the forcing locally as, for instance, in the NH only, introduce a small net global forcing. As mentioned above, this global forcing has been offset in all experiments by introducing a small change of the forcing at the lowest model level. Hence all experiments have no net global forcing and all climate responses are due solely to the redistribution of energy by the atmospheric energy transport change.

3) IMPLEMENTING ENERGY TRANSPORT FORCING

The daily climatology of the forcing is now applied online in the $1 \times CO_2$ SOM as NH, SH, and Global forcing. In addition, dry static and latent energy forcings are applied separately and in combination. In practice the model is forced by online in the model applying dry static energy and humidity tendencies [lhs of Eqs. (6) and (7)] associated with changes of the dry static and latent energy transport, respectively. For the dry static forcing, an embedded routine in the atmosphere model is used, which calculates at all model levels the temperature and geopotential-height changes in hydrostatic balance with the dry static energy change. This is, for example, the routine used for calculating temperature and geopotential height changes due to cooling and warming rates generated by the radiation code. For the latent forcing, humidity at each model level is changed corresponding to the latent transport change. To avoid nonphysical conditions with negative humidity, in the rare cases where a divergence of the latent forcing leads to a reduction of the humidity so that it would become negative, the humidity is set to zero and the remaining energy is subtracted as dry static energy following the procedure for the dry static forcing.

All runs for this study are shown in Fig. 5 for the global-mean surface air temperature (SAT) and sea ice concentration (SIC). It is seen that although the global forcing in all experiments is zero (except for the $2 \times CO_2$ experiment), many of the transport forcing experiments show considerable climate change of several degrees.

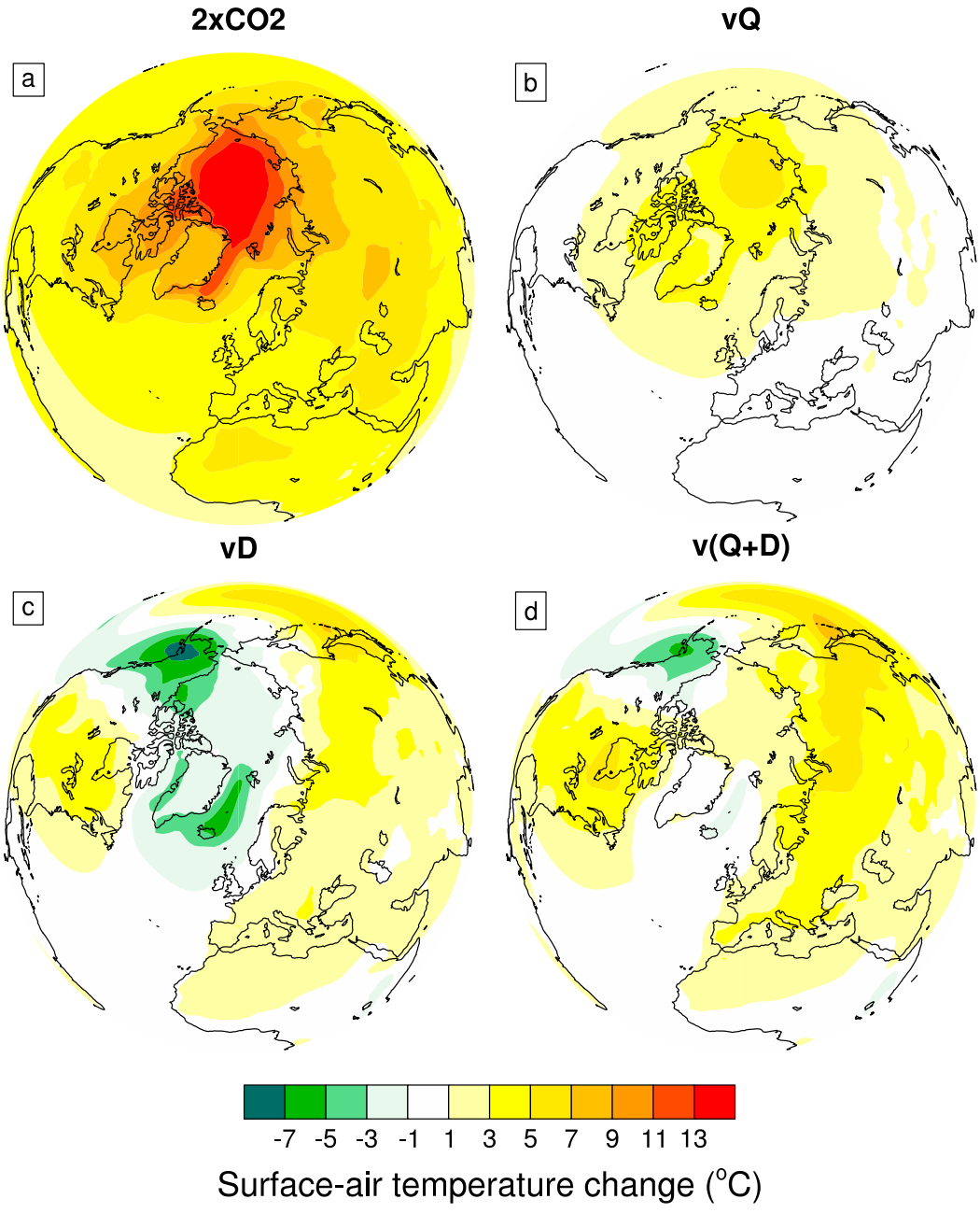

FIG. 6. Surface air temperature change due to (a) a forcing by a doubling of atmospheric CO_2, and a NH forcing by a change of the (b) latent, (c) dry static, and (d) the total energy transport divergence associated with a CO_2 doubling.

Climatologies of various quantities from the forcing experiments, and comparison of these with similar quantities from the control experiment are shown in Figs. 6–10. These climatologies are based on the last 40 years of a total of 60 years of simulation.

Note that the construction of the forcings includes several necessary steps with aspects of subjectivity as outlined above. Also the response to the energy transport forcing may be dependent on the background climate, and the forcing of a $1 \times CO_2$ climate as applied here may induce a different response as compared to the response of the same forcing during global warming of today.

In addition, the energy transport variability is correlated with other weather and climate variability patterns that may affect the response: As an example, in reality regions of divergence and convergence of the latent transport may coincide with anomalously humid and dry

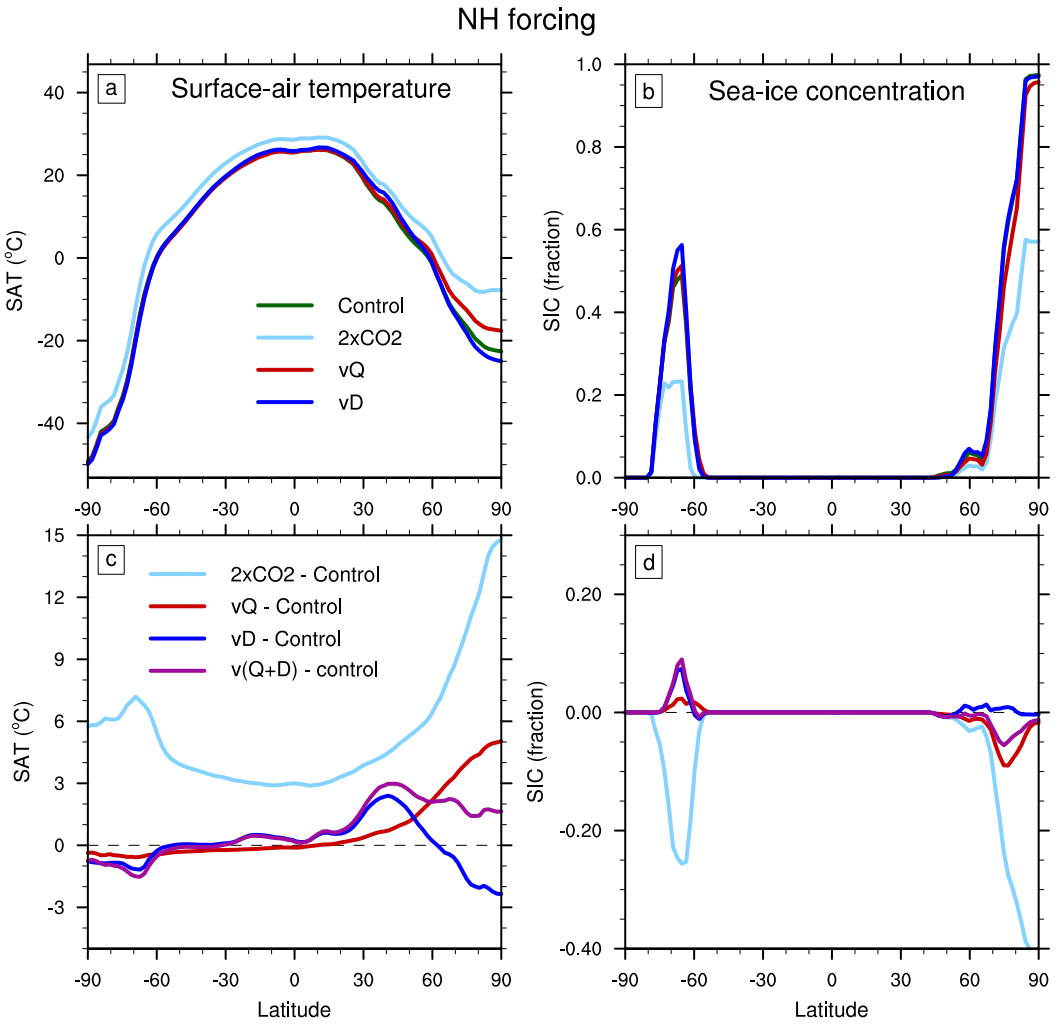

FIG. 7. (top) Climatologies as a function of latitude of (a) surface air temperature and (b) sea ice extent in the control run and experiments with a forcing from a doubling of the atmospheric CO_2 content ($2 \times CO_2$), and NH forcing by a change of latent (vQ) and dry static (vD) energy transport divergence associated with a CO_2 doubling. (bottom) Differences between forcing and control experiments are for (c) surface air temperature and (d) sea ice extent. Also shown in (c) and (d) are differences between forcing from a change of total energy transport divergence [v(Q + D)] and the control experiment.

conditions, respectively. Such a correlation affects the local greenhouse effect and hence the response. This is because the greenhouse effect of a clear-sky atmosphere to a first order is linearly dependent on the logarithm of the specific humidity (Raval and Ramanathan 1989) implying that the greenhouse effect associated with a given humidity change is dependent on the background humidity. This correlation between latent transport divergences and background humidity is missing in the experiments.

Finally, the approaches mentioned in the introduction section based on online locking of feedback processes in models differ from that in our study where the energy transport change is implemented as a forcing. It appears overly complicated to actually lock the energy transport in the model, and the choice of implementing the transport change as a forcing is here chosen as a technically realistic alternative that in many aspects is similar to the locking approach. The advantage of locking feedbacks in models is that the climate effect of the process in question can be estimated directly. In our study, where the atmospheric energy transport change is implemented as a forcing, the transport in itself may change as a consequence of the induced climate change. Hence in our study, the investigated feedback is not locked and will to some extent change and affect the response. For that reason and because of other caveats, some of those mentioned above, only general patterns of

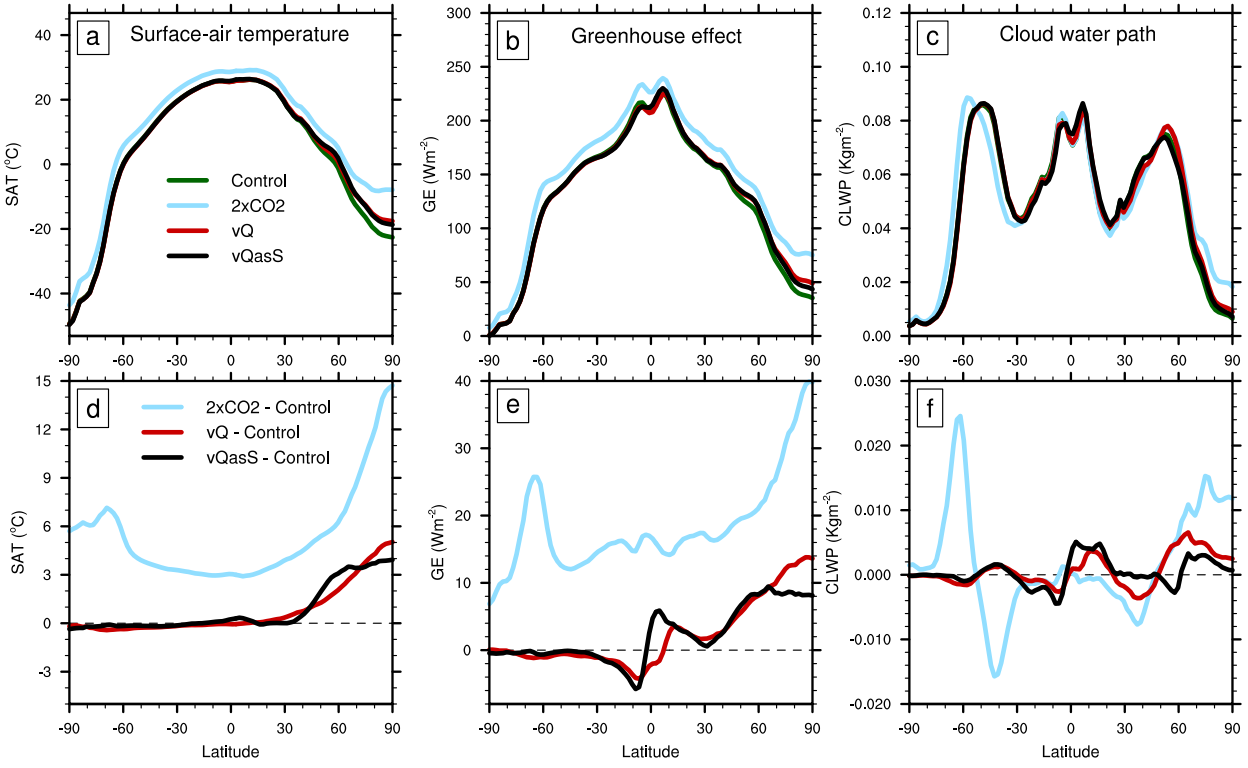

FIG. 8. As in Fig. 7, but for the (a),(d) surface air temperature, (b),(e) greenhouse effect, and (c),(f) cloud water path, and for the control, $2 \times CO_2$, and vQ NH forcing experiments. Also shown is an experiment where the vQ forcing is implemented as dry static energy rather than water vapor (vQasS). The greenhouse effect is defined as the difference between upward longwave radiation at the surface and at TOA (e.g., Raval and Ramanathan 1989). The cloud water path includes both liquid and frozen condensates.

climate response to transport forcings will be discussed, and absolute magnitudes and their comparison to the response to $2 \times CO_2$ forcing should be interpreted with caution.

Also note that the energy transport change due to a CO_2 forcing is here based on slab-ocean experiments where ocean circulation is kept fixed. Had the ocean circulation been free to change, it might, to some extent, have affected the CO_2 response as well as the climate feedbacks and the atmospheric circulation changes.

3. Energy transport change due to a CO_2 doubling

A radiative forcing of the model by a doubling of the atmospheric CO_2 content leads to global warming that is amplified in the polar regions (Figs. 6a and 7a,c). It also leads to a change of the energy transport (Fig. 1), so that the dry static transport decreases at the polar boundary whereas the latent transport increases as indicated for the Arctic boundary (70°N) by the numbers in the frame of Fig. 1b. These transport changes, arising from a changed atmospheric circulation in the model, are consistent with an intuitive explanation based on a simple diffusion relation between gradients and transports with a decreasing temperature gradient, and an increasing humidity gradient toward the equator due to global warming (e.g., North 1975). The temperature change due $2 \times CO_2$ shows polar amplification causing a reduction of the equatorward meridional temperature gradient, and due to the Clausius–Clapeyron exponential dependence of saturated water vapor pressure on temperature, a global warming is expected to induce larger humidity change at low latitudes relative to at high latitudes, causing an enhancement of the humidity gradient equatorward.

At most of the high latitudes, the changes of the two transport components are on the order of 10% relative to the control run, and the signs of the changes at the Arctic boundary are consistent with other model results (Hwang et al. 2011; Koenigk et al. 2013). The energy transport change leads to a redistribution of energy and water vapor across latitudes, thereby altering the regional SAT response to a CO_2 doubling. The transport change may even act as a global climate feedback, for instance, by affecting the surface albedo feedback associated with a change of sea ice and solar energy uptake by the climate system, and by affecting the cloud and water vapor distribution, thereby altering feedbacks

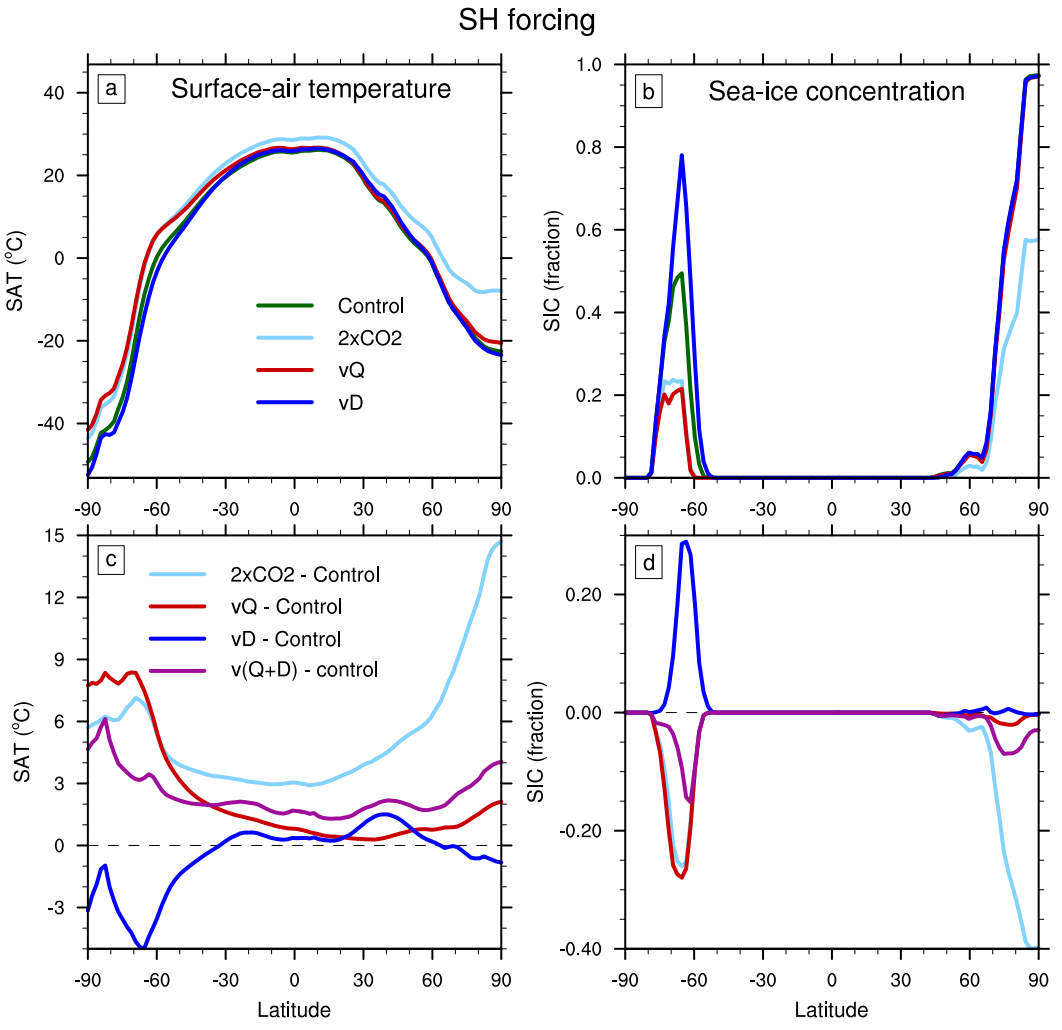

FIG. 9. As in Fig. 7 but for SH forcing from changes of energy transport divergences.

associated with these variables since their radiative forcing is dependent on location: As mentioned earlier, clouds over sea ice normally have a warming effect although clouds globally have a cooling effect (Intrieri et al. 2002). In addition, the greenhouse effect is approximately dependent on the logarithm of the specific humidity (Raval and Ramanathan 1989). Hence a transport of clouds and water vapor between different regions with different surface conditions and background humidity may alter the overall global radiative balance and therefore the global forcing of clouds and humidity. In the following, the climate response to a redistribution of dry static and latent energy will be investigated.

4. Energy transport forcing

A forcing of the model with the NH dry static energy transport change due to a CO_2 doubling leads to a cooling of the Arctic and a warming of the NH midlatitudes (Figs. 6c and 7a,c) consistent with a decrease of this transport component at the Arctic boundary. The corresponding latent transport change causes a warming of the Arctic because of a positive transport change at the lateral boundary of this region (Figs. 6b and 7a,c).

The magnitude of the Arctic cooling by the dry static transport is smaller than the warming of its latent counterpart (Fig. 7c). Consistently, if the model is forced with both components simultaneously, the response to the total energy transport change induces Arctic warming (Fig. 7c), even though the total transport change is negative at the Arctic boundary because of a larger decrease of the dry static transport compared to the increase of the latent (Fig. 1b). The convergence of the latent transport results in an enhancement of the atmospheric water vapor content and cloudiness that increases the greenhouse effect. To show this an

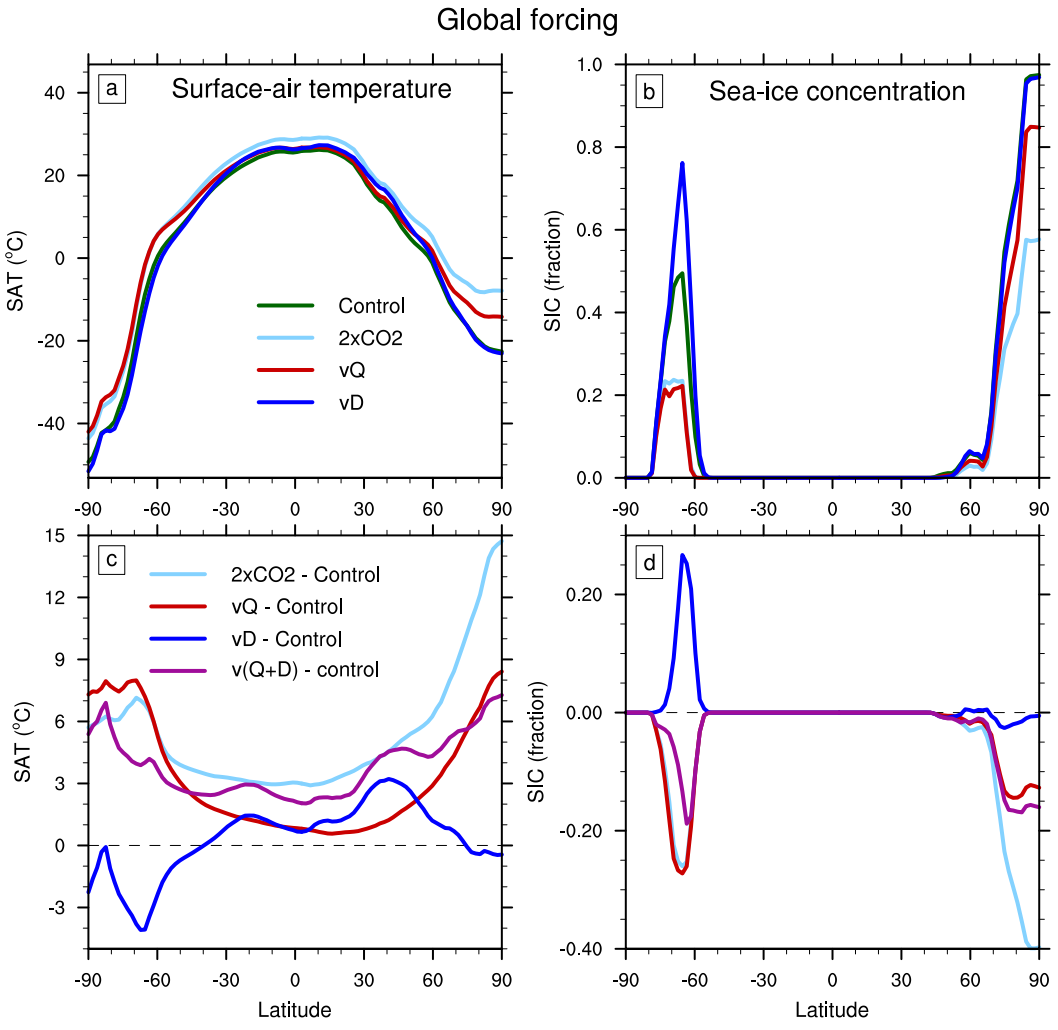

FIG. 10. As in Fig. 7 but for global forcing from changes of energy transport divergences.

experiment is conducted where the latent forcing as indicated in Fig. 3a is implemented as dry static forcing affecting only temperatures and geopotential height, instead of directly the humidity. Hereby the response to latent and dry static energy transports can be directly compared. A comparison of this experiment with the original latent forcing experiment shows that the latter experiment induces more Arctic cloudiness and a larger greenhouse effect as compared to a similar forcing implemented as dry static energy (Fig. 8). Here the greenhouse effect is defined as difference in upward longwave radiation at the surface and TOA.

In addition, the Arctic warming by the latent forcing induces a reduction of the Arctic sea ice (Figs. 7b,d) that through the albedo effect likely enhances the Arctic warming response. In contrast, the Arctic cooling due to the dry static forcing has only little effect on the sea ice. Both the stronger greenhouse effect and stronger sea ice albedo effect associated with the latent forcing as compared to the dry static forcing are consistent with the Arctic temperature response being larger for the latent transport than for the dry static.

The forcing due to changes of the two transport components in the SH shows a similar latitudinal pattern as that in the NH (Fig. 3). However, the forcing at the high latitudes is larger in magnitude in the SH forcing experiment than in that of the NH. In addition, the sea ice conditions in the SH are different from those in the NH, in particular because of the different distribution of continents in the two hemispheres. In the NH, the Arctic Ocean is bounded toward the south by continents and relatively warm water, especially in the Atlantic sector, which causes restrictions on the southward growth of the ice (Eisenman 2010). In contrast in the SH, the sea ice around Antarctica is situated at lower latitudes as compared to the NH (e.g., Fig. 9b), in a cold circumpolar

ocean where it may more easily than in the NH grow equatorward in response to cold climate perturbations. Hence the ice albedo feedback acts more strongly in the SH as compared to the NH. As a result the overall latitudinal temperature response to the SH forcing is similar in shape but larger in magnitude at the high latitudes for the SH case compared to the NH (Figs. 7 and 9).

The latent SH forcing causes warming over the Antarctic region to the extent that this warming leads to considerable global warming in this experiment (Fig. 5), which is amplified also in the NH (Fig. 9c). The reduction of sea ice in the SH caused by the latent SH forcing is similar in magnitude to that in the $2 \times CO_2$ experiment. The cooling over the SH sea ice areas due to the dry static SH forcing has likewise a pronounced effect on the sea ice, in contrast to the dry static NH forcing that affected Arctic sea ice only little. As mentioned above, this is likely an effect of the difference in continental distribution in the two hemispheres and the consequently much larger potential for ice growth in the SH as compared to the NH. Similar to the NH, the total energy transport change in the SH leads to a warming of the Antarctic region.

When global energy transport forcing is considered, there is a clear polar amplification of the total forcing that is linked to the latent transport but partly offset by the dry static (Fig. 10). The pattern is similar to the sum of the responses to the separate forcings of the two hemispheres. The total forcing induces warming at all latitudes that is partly amplified by the sea ice albedo effect at the high latitudes. Hence the energy transport acts both as a redistribution mechanism of the $2 \times CO_2$ warming and as a global climate feedback that alters the global mean response.

5. Conclusions

A method has been developed to estimate the 3D energy transport divergence pattern in a coordinate system where pressure at vertical hybrid levels varies in time and horizontal space. Such coordinate systems are often applied in climate models and in particular in the CESM model. For the dry static energy transport, there is an intrinsic linkage between horizontal and vertical components that has to be taken into account when considering the forcing associated with the change of this transport component.

In the CESM model, the 3D change in transport divergences due to a CO_2 doubling is used as a forcing of the $1 \times CO_2$ preindustrial climate in order to separately estimate the climate effect of this transport change. Note that in all experiments the global-mean forcing is zero, so that any global response is solely a result of redistributing of energy within the atmosphere.

When transport changes in the NH are considered, it is found that in the Arctic, the change of the latent energy transport causes a warming that more than compensates a cooling due to the dry static transport change (Fig. 7). Hence in total, the change of the energy transport leads to a warming of the Arctic despite the fact that the transport change at the Arctic boundary is negative. This is consistent with earlier results based on different methods (Graversen and Burtu 2016; Yoshimori et al. 2017), and in opposition to, for example, Kay et al. (2012) arguing that energy transport, if decreasing at the Arctic boundary, cannot play a contributing role for Arctic amplification. The decrease in total transport leads to a warming due to a shift between the two transport components, so that the dry static transport decreases and the latent transport increases. The latent transport brings to the Arctic not only energy but also water vapor, which in itself and through the formation of clouds enhances the local Arctic greenhouse effect (Fig. 8).

The transport change in the SH has a similar latitudinal structure compared to that in the NH, but according to the CESM model the change of the transport leads to larger divergences and convergences in the SH as compared to the NH (Fig. 3). Consistently, the energy transport causes a similar response in the SH as in the NH, but with larger magnitudes. The energy transport leads to a considerable warming of the Antarctic area resulting in strong sea ice melt that likely further enhances the warming through the ice albedo feedback. Hereby the SH forcing leads to global warming that is even slightly amplified in the NH (Fig. 9).

Although several simplifications and assumptions were made in order to implement the effect of atmospheric energy transport change as a forcing, we believe that the fundamental idea of the experiment is sound: The effect of the dry static energy transport change is implemented similar to the way the model takes into account a change in electromagnetic energy radiation such as a change in solar radiation. As mentioned earlier, the latent energy transport change is implemented by altering the humidity directly, but an experiment where this transport change is implemented similar to that of the dry static reveals a difference in response between the two ways of implementing the transport that is consistent with the greenhouse effect of the transported water vapor being included in the former method but ignored in the latter (Fig. 8). Hence these model results, despite all assumptions, indicate that the energy transport may play a large role in climate change,

not only by redistributing energy but also by contributing to global warming, for instance, by triggering other climate feedbacks such as the ice albedo feedback. Finally, the results here show that change in poleward energy transport, even if decreasing may contribute to polar temperature amplification.

Acknowledgments. The work is funded by The Research Council of Norway (NFR) as part of the project ''The role of the atmospheric energy transport in recent Arctic climate change'' with project number 280727. The CESM experiments were performed at the supercomputer Vilje at The Norwegian University of Science and Technology (NTNU) under the Norwegian Metacenter for Computational Science (NOTUR) project NN9348K and NS9063. CESM was obtained from NCAR, Boulder, Colorado, United States. We thank three anonymous reviewers for constructive and useful suggestions.

REFERENCES

Alexeev, V. A., P. L. Langen, and J. R. Bates, 2005: Polar amplification of surface warming on an aquaplanet in ''ghost forcing'' experiments without sea ice feedbacks. *Climate Dyn.*, **24**, 655–666, https://doi.org/10.1007/s00382-005-0018-3.

Bengtsson, L., K. Hodges, S. Koumoutsaris, M. Zahn, and P. Berrisford, 2013: The changing energy balance of the polar regions in a warmer climate. *J. Climate*, **26**, 3112–3129, https://doi.org/10.1175/JCLI-D-12-00233.1.

Bitz, C. M., K. M. Shell, P. R. Gent, D. A. Bailey, G. Danabasoglu, K. C. Armour, M. M. Holland, and J. T. Kiehl, 2012: Climate sensitivity of the Community Climate Model version 4. *J. Climate*, **25**, 3053–3070, https://doi.org/10.1175/JCLI-D-11-00290.1.

Cai, M., 2005: Dynamical amplification of polar warming. *Geophys. Res. Lett.*, **32**, L22710, https://doi.org/10.1029/2005gl024481.

Dahlke, S., and M. Maturilli, 2017: Contribution of atmospheric advection to the amplified winter warming in the Arctic North Atlantic region. *Adv. Meteor.*, **2017**, 4928620, https://doi.org/10.1155/2017/4928620.

Ding, Q., and Coauthors, 2017: Influence of high-latitude atmospheric circulation changes on summertime Arctic sea ice. *Nat. Climate Change*, **7**, 289–296, https://doi.org/10.1038/nclimate3241.

Eisenman, I., 2010: Geographic muting of changes in the Arctic sea ice cover. *Geophys. Res. Lett.*, **37**, L16501, https://doi.org/10.1029/2010GL043741.

Gong, T., S. Feldstein, and S. Lee, 2017: The role of downward infrared radiation in the recent Arctic winter warming trend. *J. Climate*, **30**, 4937–4949, https://doi.org/10.1175/JCLI-D-16-0180.1.

Graversen, R. G., 2006: Do changes in midlatitude circulation have any impact on the Arctic surface air temperature trend? *J. Climate*, **19**, 5422–5438, https://doi.org/10.1175/JCLI3906.1.

——, and M. Wang, 2009: Polar amplification in a coupled climate model with locked albedo. *Climate Dyn.*, **33**, 629–643, https://doi.org/10.1007/s00382-009-0535-6.

——, and M. Burtu, 2016: Arctic amplification enhanced by latent energy transport of atmospheric planetary waves. *Quart. J. Roy. Meteor. Soc.*, **142**, 2046–2054, https://doi.org/10.1002/qj.2802.

——, P. L. Langen, and T. Mauritsen, 2014: Polar amplification in CCSM4: Contributions from the lapse rate and surface albedo feedbacks. *J. Climate*, **27**, 4433–4450, https://doi.org/10.1175/JCLI-D-13-00551.1.

Hall, A., 2004: The role of surface albedo feedback in climate. *J. Climate*, **17**, 1550–1568, https://doi.org/10.1175/1520-0442(2004)017<1550:TROSAF>2.0.CO;2.

——, and S. Manabe, 1999: The role of water vapor feedback in unperturbed climate variability and global warming. *J. Climate*, **12**, 2327–2345, https://doi.org/10.1175/1520-0442(1999)012<2327:TROWVF>2.0.CO;2.

Hansen, J., A. Lacis, D. Rind, G. Russel, P. Stone, I. Fung, R. Ruedy, and J. Lerner, 1984: Climate sensitivity: Analysis of feedback mechanisms. *Climate Processes and Climate Sensitivity, Geophys. Monogr.*, Vol. 29, Amer. Geophys. Union, 130–163.

Hurrell, J. W., and Coauthors, 2013: The Community Earth System Model: A framework for collaborative research. *Bull. Amer. Meteor. Soc.*, **94**, 1339–1360, https://doi.org/10.1175/BAMS-D-12-00121.1.

Hwang, Y. T., D. M. W. Frierson, and J. E. Kay, 2011: Coupling between Arctic feedbacks and changes in poleward energy transport. *Geophys. Res. Lett.*, **38**, L17704, https://doi.org/10.1029/2011gl048546.

Intrieri, J. M., M. D. Shupe, T. Uttal, and B. J. McCarty, 2002: An annual cycle of Arctic cloud characteristics observed by radar and lidar at SHEBA. *J. Geophys. Res.*, **107**, 8030, https://doi.org/10.1029/2000jc000423.

Isaksen, K., Ø. Nordli, E. J. Førland, E. Łupikasza, and T. Niedźwiedź, 2016: Recent warming on Spitsbergen—Influence of atmospheric circulation and sea ice cover. *J. Geophys. Res.*, **121**, 11 913–11 931, https://doi.org/10.1002/2016jd025606.

Kapsch, M.-L., R. G. Graversen, and M. Tjernström, 2013: Springtime atmospheric energy transport and the control of Arctic summer sea-ice extent. *Nat. Climate Change*, **3**, 744–748, https://doi.org/10.1038/nclimate1884.

Kasahara, A., 1974: Various vertical coordinate systems used for numerical weather predictions. *Mon. Wea. Rev.*, **102**, 509–522, https://doi.org/10.1175/1520-0493(1974)102<0509:VVCSUF>2.0.CO;2.

Kay, J. E., M. M. Holland, C. M. Bitz, E. Blanchard-Wrigglesworth, A. Gettelman, and D. Bailey, 2012: The influence of local feedbacks and northward heat transport on the equilibrium Arctic climate response to increased greenhouse gas forcing. *J. Climate*, **25**, 5433–5450, https://doi.org/10.1175/JCLI-D-11-00622.1.

Koenigk, T., L. Brodeau, R. G. Graversen, J. Karlsson, G. Svensson, M. Tjernström, U. Willén, and K. Wyser, 2013: Arctic climate change in 21st century CMIP5 simulations with EC-Earth. *Climate Dyn.*, **40**, 2719–2743, https://doi.org/10.1007/s00382-012-1505-y.

Langen, P. L., and V. A. Alexeev, 2007: Polar amplification as a preferred response in an idealized aquaplanet GCM. *Climate Dyn.*, **29**, 305–317, https://doi.org/10.1007/s00382-006-0221-x.

——, R. G. Graversen, and T. Mauritsen, 2012: Separation of contributions from radiative feedbacks to polar amplification on an aquaplanet. *J. Climate*, **25**, 3010–3024, https://doi.org/10.1175/JCLI-D-11-00246.1.

Lee, H. J., M. O. Kwon, S.-W. Yeh, Y.-O. Kwon, W. Park, J.-H. Park, Y. H. Kim, and M. A. Alexander, 2017: Impact of

poleward moisture transport from the North Pacific on the acceleration of sea ice loss in the Arctic since 2002. *J. Climate*, **30**, 6757–6769, https://doi.org/10.1175/JCLI-D-16-0461.1.

Lee, S., T. Gong, S. B. Feldstein, J. A. Screen, and I. Simmonds, 2017: Revisiting the cause of the 1989–2009 Arctic surface warming using the surface energy budget: Downward infrared radiation dominates the surface fluxes. *Geophys. Res. Lett.*, **44**, 10 654–10 661, https://doi.org/10.1002/2017GL075375.

Mauritsen, T., R. G. Graversen, D. Klocke, P. L. Langen, B. Stevens, and L. Tomassini, 2013: Climate feedback efficiency and synergy. *Climate Dyn.*, **41**, 2539–2554, https://doi.org/10.1007/s00382-013-1808-7.

Mortin, J., G. Svensson, R. G. Graversen, M.-L. Kapsch, J. Stroeve, and L. Boisvert, 2016: Melt onset over the Arctic sea ice controlled by atmospheric moister transport. *Geophys. Res. Lett.*, **43**, 6636–6642, https://doi.org/10.1002/2016GL069330.

Neale, R. B., and Coauthors, 2012: Description of the NCAR Community Atmosphere Model (CAM 5.0). NCAR Tech. Note NCAR/TN-486+STR, 274 pp., www.cesm.ucar.edu/models/cesm1.0/cam/docs/description/cam5_desc.pdf.

North, G. R., 1975: Analytical solution to a simple climate model with diffusive heat transport. *J. Atmos. Sci.*, **32**, 1301–1307, https://doi.org/10.1175/1520-0469(1975)032<1301:astasc>2.0.co;2.

Oort, A. H., and J. P. Peixóto, 1983: Global angular momentum and energy balance requirements from observations. *Advances in Geophysics*, Vol. 25, Academic Press, 355–490, https://doi.org/10.1016/S0065-2687(08)60177-6.

Raval, A., and V. Ramanathan, 1989: Observational determination of the greenhouse effect. *Nature*, **342**, 758–761, https://doi.org/10.1038/342758a0.

Schneider, E. K., B. P. Kirtman, and R. S. Lindzen, 1999: Tropospheric water and climate sensitivity. *J. Atmos. Sci.*, **56**, 1649–1658, https://doi.org/10.1175/1520-0469(1999)056<1649:TWVACS>2.0.CO;2.

Skific, N., and J. Francis, 2013: Drivers of projected change in Arctic moist static energy transport. *J. Geophys. Res. Atmos.*, **118**, 2748–2761, https://doi.org/10.1002/jgrd.50292.

Soden, B. J., I. M. Held, R. Colman, K. M. Shell, J. T. Kiehl, and C. A. Shields, 2008: Quantifying climate feedbacks using radiative kernels. *J. Climate*, **21**, 3504–3520, https://doi.org/10.1175/2007JCLI2110.1.

Vavrus, S., 2004: The impact of cloud feedbacks on Arctic climate under greenhouse forcing. *J. Climate*, **17**, 603–615, https://doi.org/10.1175/1520-0442(2004)017<0603:TIOCFO>2.0.CO;2.

Wetherald, R. T., and S. Manabe, 1988: Cloud feedback processes in a general circulation model. *J. Atmos. Sci.*, **45**, 1397–1415, https://doi.org/10.1175/1520-0469(1988)045<1397:CFPIAG>2.0.CO;2.

Woods, C., and R. Caballero, 2016: The role of moist intrusions in winter Arctic warming and sea ice decline. *J. Climate*, **29**, 4473–4485, https://doi.org/10.1175/JCLI-D-15-0773.1.

——, ——, and G. Svensson, 2013: Large-scale circulation associated with moisture intrusions into the Arctic during winter. *Geophys. Res. Lett.*, **40**, 4717–4721, https://doi.org/10.1002/grl.50912.

Yang, W., and G. Magnusdottir, 2017: Springtime extreme moisture transport into the Arctic and its impact on sea ice concentration. *J. Geophys. Res. Atmos.*, **122**, 5316–5329, https://doi.org/10.1002/2016JD026324.

Yoshimori, M., A. Abe-Ouchi, and A. Laîné, 2017: The role of atmospheric heat transport and regional feedbacks in the Arctic warming at equilibrium. *Climate Dyn.*, **49**, 3457–3472, https://doi.org/10.1007/s00382-017-3523-2.